# Computation of Broadband Noise Radiated by a Ducted Fan in a Uniform Flow

**Serge Lewy**[†]

*Office National d'Etudes et de Recherches Aérospatiales (ONERA), MB 72, 92322 Chatillon, France*

(Received 30 July 2003; accepted 20 October 2003)

Ducted-fan broadband noise often dominates overall sound levels radiated by a modern aircraft high-bypass-ratio turbofan at subsonic rotational tip speeds. As a result, its prediction has become a challenge for additional noise reduction. Equations were established in a previous work for a uniform flow inside the duct, the free medium being at rest (case of static tests). However, induct and free-field acoustic powers are not balanced if there is a flow mismatch at the duct exit. Free-field computation is thus extended to a medium in translation which better simulates flight conditions (the same velocity being taken throughout the space). The radiation model of Tyler and Sofrin (Rayleigh's integral) is no longer valid, and a routine based on the Kirchhoff integral equation has been implemented. It is checked that all the previous results are verified, both in the no-flow case and with flow only inside the duct. Computations assuming a uniform flow throughout the space now lead to the same acoustic power inside the duct and in the free field. This is a basic validation of the prediction model. It is mainly found that flow velocity tends to increase rotor forward radiation and to decrease aft radiation.

[†] Member of the International Institute of Acoustics and Vibration (IIAV)

## Notations

$a$ – Speed of sound
$A_{m\mu}$ – Modal amplitude of induct acoustic pressure
$c$ – Blade chord
$(D, \theta, \phi)$ – Spherical coordinates in the free field
$D', \hat{d}$ – Modified distances
$F$ – Blade loading
$f$ – Frequency
$\vec{\mathrm{I}}$ – Acoustic intensity
$\mathrm{J}_m$ – Bessel function of the first kind, and of order $m$
$K, k_t, k_z$ – Total, transverse, and axial wave-numbers
$M_z$ – Axial Mach number,
$m, \mu$ – Circumferential and radial modes
$N$ – Rotational speed
$p, p_d$ – Free-field and induct acoustic pressure
$P_0$ – Amplitude of free-field acoustic pressure
$R$ – Duct radius
$(r, \varphi, z)$ – Cylindrical coordinates inside the duct
$t$ – Reception time
$U_{hel}$ – Helical velocity on a rotor blade ($U_{hel} = aM_{hel}$)
$U_0$ – Mean flow velocity ($U_0 = aM_z$)
$\vec{\mathrm{u}}$ – Acoustic velocity
$v$ – Disturbance velocity normal to a blade
$\alpha$ – Flow angle of attack on the rotor blades
$\beta, \beta_\theta$ – Factors of axial Mach number, see Eqs. (4)
$\rho_0$ – Fluid mean density
$\sigma$ – Modified distance
$\tau$ – Retarded time
$\Phi$ – Fourier transform of the blade loading
$\Psi$ – Directivity factor of the radiated acoustic field
$\omega$ – Angular frequency ($\omega = 2\pi f = aK$)

## Abbreviations

OAPWL – Overall sound power level
OASPL – Overall sound pressure level
PWL – Sound power level
T&S – Tyler and Sofrin, see reference 5

## 1. INTRODUCTION

Fan broadband noise often is the major component of overall sound levels radiated by aircraft turbofans at subsonic rotation speeds due to past progress in decreasing the tones. Its prediction has thus become a new challenge for further noise reduction. Forward radiation is mainly due to fluctuating blade pressure (either self-noise, or interaction with incoming turbulence). Computational fluid dynamics (CFD) is not yet able to predict random loads on rotating airfoils, and tests using blade pressure transducers are very expensive. Thus, semi-empirical modelling is still being developed.[1]

A prediction method based on analytic equations is a middle way that was proposed in a previous work (see Fig. 1).[2] It is based on the model of Ffowcs Williams and Hawkings of a random rotating dipole,[3] and their equation is modified to take into account the Green's function inside a hard-walled infinite cylindrical duct.[4] Free-field radiation is then calculated using Tyler and Sofrin's (T&S) model (Rayleigh's integral).[5] This approach only requires the blade pressure spectrum, assumed to be known, whatever its source may be. An important hypothesis is that there is no reflection on the duct exit, but this is more or less valid except at low frequencies.[6] Equations were derived for a uniform flow inside the duct and for the free medium at rest (case of static tests). Flow inside the duct was however neglected in the results of reference 2 to balance acoustic powers in the duct and in the free field. Indeed, the hypotheses in the acoustic equations used inside the duct and in the free field were different, due to the flow mismatch at the duct exit.

This paper shows how free-field computation can be extended to a medium in translation which better simulates flight conditions (the same velocity being taken throughout the space). The simple radiation model of T&S is no longer valid, and a routine based on the full Kirchhoff integral equation is described in the next section. Some results are then discussed for a model fan tested by Rolls-Royce within the framework of the FANPAC (Fan-Noise Prediction and Control) European project.

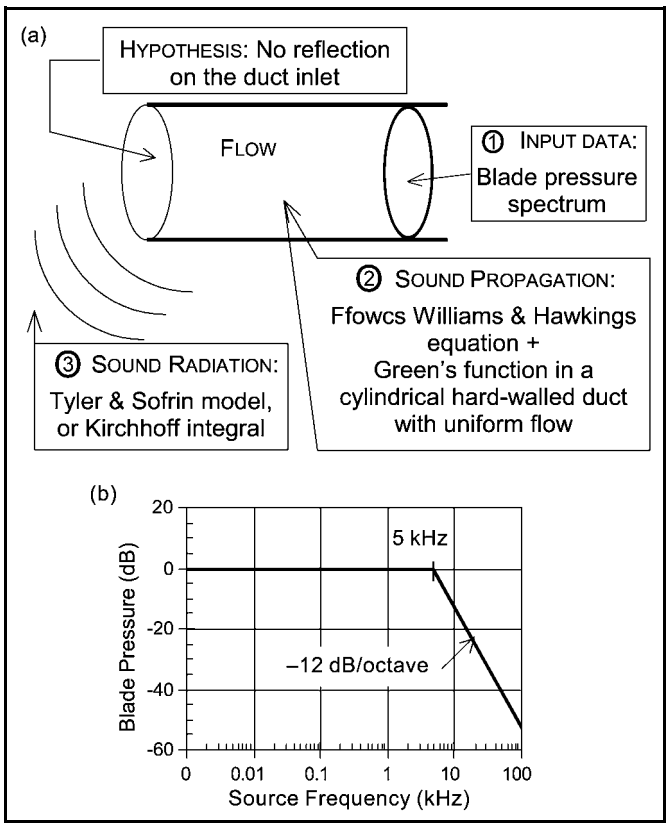


**Figure 1.** Prediction method (a), and shape of the input blade pressure spectrum (b).

## 2. RADIATION FROM THE INTAKE OF A CYLINDRICAL DUCT

Let us consider a cylindrical duct of radius $R$ (Fig. 2). Space is referred to Cartesian coordinates $(x,y,z)$. Cylindrical coordinates $(r,\varphi,z)$ are used inside the duct, and spherical coordinates $(D,\theta,\phi)$ are used in the free field. The origin O of the two systems is located on the centre of the duct exit cross-section. The fluid is in uniform translation both inside the duct and in the free field. The same velocity is taken throughout the space to avoid any flow mismatch in the exit plane: $U_0 = aM_z$ is positive along the $z$-axis ($a$ is the speed of sound, and $M_z$ is the Mach number). Possible reflections of incident acoustic waves on the duct exit are neglected.

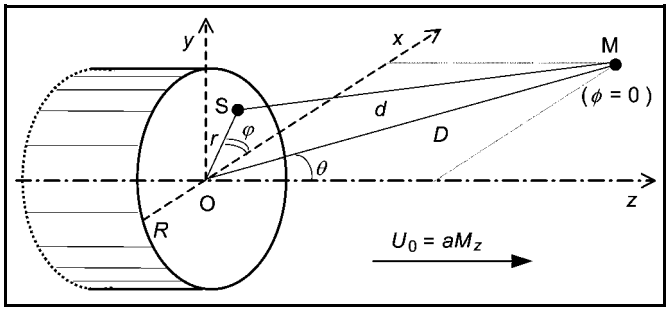


**Figure 2.** Diagram of the duct geometry and of the coordinate systems.

Induct sound pressure at a given angular frequency $\omega = 2\pi f = aK$ ($f$ is the frequency, and $K$ is the total wave-number) can be split into spinning modes $(m,\mu)$. For a single mode:

$$p_d(r,\varphi,z,t) = A_{m\mu} \mathrm{J}_m(k_t r) e^{i(\omega t - m\varphi - k_z z)}, \tag{1}$$

where $m$ and $\mu$ being the azimuthal and radial modes; $k_t$ and $k_z$ are the transverse and axial wave-numbers, respectively, and $\mathrm{J}_m$ is the Bessel function of the first kind and of order $m$. Equation connecting amplitude $A_{m\mu}$ to blade thrust and drag was derived in reference 2.

### 2.1. Acoustic Radiation in a Fluid in Translation

Kirchhoff formula neglecting the near-field term is the integral of the following equation over the exit cross-section:[7]

$$\delta p(D,\theta,\phi,t) = \frac{1}{4\pi\hat{d}}\left[(1-M_z^2)\frac{\partial}{\partial z} - \frac{1}{a}\left(\frac{z_M}{\hat{d}} + M_z\right)\frac{\partial}{\partial \tau}\right] \times p_d(r,\varphi,z,\tau)_{z=0}\,\delta S, \tag{2}$$

where $z_M$ is the abscissa of the observer M, and $\tau = t - \sigma/a$ is the retarded time. The lengths $\hat{d}$ and $\sigma$ are the modified distances from a point source S to M in a uniform flow.

As the geometry is axisymmetric, the x-axis can lie in the $z$OM plane such that $\phi = 0$ which simplifies the equations without any loss of generality:

$$\left.\begin{array}{ll} \mathrm{S} & (x_S = r\cos\varphi, \quad y_S = r\sin\varphi, \quad z_S = 0), \\ \mathrm{M} & (x_M = D\sin\theta, \quad y_M = 0, \qquad z_M = D\cos\theta). \end{array}\right\} \tag{3}$$

If we put:

$$\beta^2 = 1 - M_z^2, \text{ and } \beta_\theta^2 = 1 - M_z^2\sin^2\theta, \tag{4}$$

equations for $\hat{d}$ and $\sigma$ become as follows:

$$\hat{d}^2 = \beta^2(x_M - x_S)^2 + \beta^2(y_M - y_S)^2 + (z_M - z_S)^2,$$

or

$$\hat{d} = \beta_\theta D\left(1 - 2\frac{\beta^2}{\beta_\theta^2}\frac{r}{D}\sin\theta\cos\varphi + \frac{\beta^2}{\beta_\theta^2}\frac{r^2}{D^2}\right)^{1/2}, \tag{5a}$$

and

$$\sigma = \frac{\hat{d} - M_z(z_M - z_S)}{\beta^2} = \frac{\hat{d} - M_z D\cos\theta}{\beta^2}, \tag{6a}$$

This leads to the far-field approximation:

$$\hat{d} \approx \beta_\theta D - \frac{\beta^2}{\beta_\theta} r\sin\theta\cos\varphi, \tag{5b}$$

and

$$\sigma \approx D' - \frac{r}{\beta_\theta}\sin\theta\cos\varphi, \tag{6b}$$

with

$$D' = \frac{\beta_\theta - M_z\cos\theta}{\beta^2} D, \tag{7}$$

where $D'$ is independent of the source coordinates. One must ensure that $0 \le \theta \le \pi/2$ for downstream radiation, and $\pi/2 \le \theta \le \pi$ for upstream radiation, due to the fact that $U_0$ and $M_z$ are taken to be positive.

Equation (2) becomes due to Eq. (1):

$$\delta p(D,\theta,t) = \frac{-iA_{m\mu}}{4\pi\hat{d}}\left[\beta^2 k_z + \left(\frac{D\cos\theta}{\hat{d}} + M_z\right)K\right] \times \mathrm{J}_m(k_t r) e^{i\omega(t-\sigma/a) - im\varphi}\,\delta S. \tag{8}$$

It can be put $\widehat{d} \approx \beta_\theta D$ in the multiplying factors according to Eq. (5b), but the first-order term of Eq. (6b) must be kept in the phase $e^{-i\omega\sigma/a}$:

$$\delta p(D,\theta,t) = \frac{-iP_0}{\pi RD} \mathrm{J}_m(k_t r) e^{i\omega(t-D'/a)} e^{i(Kr/\beta_\theta)\sin\theta\cos\varphi - im\varphi} \delta S, \quad (9)$$

with the amplitude

$$P_0 = \frac{A_{m\mu} R}{4\beta_\theta}\left[\beta^2 k_z + \left(\frac{\cos\theta}{\beta_\theta} + M_z\right)K\right]. \quad (10)$$

The integration on $\delta S = r\,dr\,d\varphi$ in the circle of radius $R$ can be made analytically using the relations of Bessel functions. First integration on angle $\varphi$ leads to:

$$p(D,\theta,t) = \frac{2P_0}{RD} i^{m-1} e^{i\omega(t-D'/a)} \int_0^R \mathrm{J}_m(k_t r)\mathrm{J}_m\left(\frac{Kr}{\beta_\theta}\sin\theta\right) r\,dr. \quad (11)$$

Assuming that the duct wall is perfectly rigid, i.e., the derivative $\mathrm{J}'_m(k_t R) = 0$, the final result is:

$$p(D,\theta,t) = \frac{P_0 R}{D} i^{m-1} e^{i\omega(t-D'/a)} \mathrm{J}_m(k_t R)\Psi(\theta), \quad (12a)$$

the directivity factor, $\Psi(\theta)$, being

$$\Psi(\theta) = \frac{2(KR/\beta_\theta)\sin\theta}{(k_t R)^2 - [(KR/\beta_\theta)\sin\theta]^2} \mathrm{J}'_m\left(\frac{KR}{\beta_\theta}\sin\theta\right). \quad (13)$$

If $\sin\theta = \beta_\theta k_t / K$, then:

$$p(D,\theta,t) = \frac{P_0 R}{D} i^{m-1} e^{i\omega(t-D'/a)}\left(1 - \frac{m^2}{k_t^2 R^2}\right)\mathrm{J}_m^2(k_t R). \quad (12b)$$

### 2.2. Acoustic Intensity Radiated in the Free Field

A basic assessment of the validity of the computations consists in checking that sound powers inside the duct and radiated in the far field are equal. Equations in the duct have been derived in reference 2. The sound power in free field is deduced from integration of the radial component of the time-averaged sound intensity computed on a sphere of radius $D$. The sound intensity in a uniform flow of velocity $U_0 = aM_z$ is given by Cantrell and Hart:[8]

$$\vec{\mathrm{I}} = \left[p + \rho_0\left(\vec{\mathrm{U}}_0 \cdot \vec{\mathrm{u}}\right)\right]\left(\vec{\mathrm{u}} + \frac{p}{\rho_0 a^2}\vec{\mathrm{U}}_0\right), \quad (14)$$

where $\rho_0$ is the mean fluid density, and $\vec{\mathrm{u}}$ is the acoustic velocity. Thus the radial components $u$ of $\vec{\mathrm{u}}$, and $I$ of $\vec{\mathrm{I}}$ are:

$$I = (p + \rho_0 a u M_z\cos\theta)\left(u + \frac{p}{\rho_0 a}M_z\cos\theta\right)$$

$$= (1 + M_z^2\cos^2\theta)pu + (M_z\cos\theta)\left(\frac{p^2}{\rho_0 a} + \rho_0 a u^2\right). \quad (15)$$

The momentum equation links $u$ to $p$:

$$\rho_0\frac{d\vec{\mathrm{u}}}{dt} + \vec{\nabla}p = \vec{0},$$

with its radial component

$$\rho_0\left(iaKu + aM_z\frac{\partial u}{\partial z}\right) + \frac{\partial p}{\partial D} = 0. \quad (16)$$

The derivatives are computed from Eq. (12a), neglecting the terms in $1/D^2$ compared with $1/D$ in the far field:

$$\rho_0 a\left(iKu - M_z iKu\frac{\partial D'}{\partial z}\right) - iKp\frac{\partial D'}{\partial D} = 0,$$

or

$$\rho_0 a\left(1 - M_z\frac{\partial D'}{\partial z}\right)u = \frac{\partial D'}{\partial D}p. \quad (17)$$

According to Eq. (7), it comes:

$$\frac{\partial D'}{\partial D} = \frac{\beta_\theta - M_z\cos\theta}{\beta^2}. \quad (18a)$$

and

$$\frac{\partial D'}{\partial z} = \frac{\partial D'}{\partial D}\frac{\partial D}{\partial z},$$

or

$$\frac{\partial D'}{\partial z} = \frac{\beta_\theta - M_z\cos\theta}{\beta^2}\frac{\partial D}{\partial z}, \text{ with } \frac{\partial D}{\partial z} = \frac{z_M}{D} = \cos\theta. \quad (18b)$$

Finally:

$$\rho_0 a u = p/\beta_\theta, \quad (19)$$

($\beta_\theta$ is close to 1, and equal to 1 without flow), and Eq. (15) becomes:

$$I = \left[\frac{1 + M_z^2\cos^2\theta}{\beta_\theta} + \left(1 + \frac{1}{\beta_\theta^2}\right)M_z\cos\theta\right]\frac{p^2}{\rho_0 a}. \quad (20)$$

## 3. COMPUTATIONAL RESULTS

The above equations are applied to tests run by Rolls-Royce in their Ansty noise compressor test facility (ANCTF) within the framework of the European project FANPAC.[9] The main characteristics of the model fan are: diameter $2R = 0.864$ m, 24 blades, hub-to-tip ratio = 0.391, design rotation speed 10,100 rpm. The blade pressure spectrum is assumed to be flat over a large frequency range according to several available tests (Fig. 1(b)). We make it decrease towards high frequencies in such a way that the overall fluctuations remain finite. Its amplitude has been chosen to get realistic sound levels, but no attempt was made to accurately match actual experimental sound levels.

### 3.1. Results Without Flow

First of all, one must check if the Kirchhoff method gives the same results as the T&S radiation model without flow. Fig. 3 shows the forward directivity patterns of overall sound

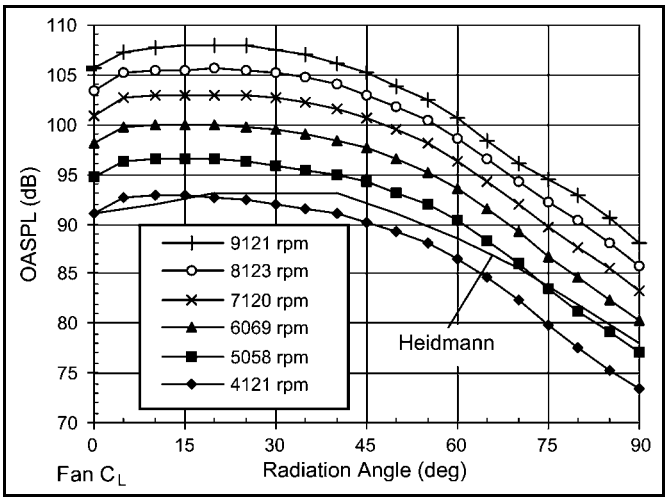


**Figure 3.** Upstream directivities: Kirchhoff integral, no flow.

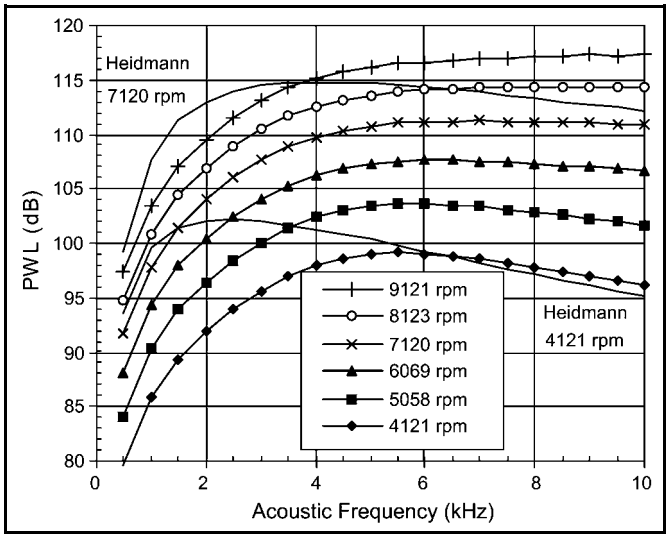


**Figure 4.** Upstream sound power spectra: Kirchhoff integral, no flow.

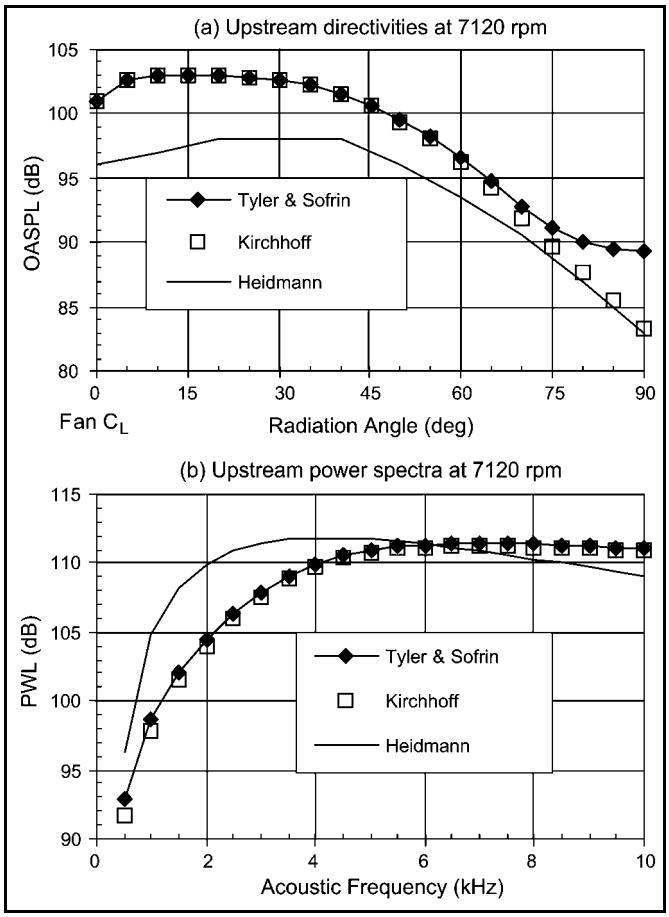


**Figure 5.** Upstream directivities and sound power spectra at 7120 rpm: Comparisons of Tyler and Sofrin, Kirchhoff, and semi-empirical methods.

pressure levels (OASPL) integrated from 500 Hz to 10 kHz, for several rotation speeds (radiation angle is here $\pi - \theta$). The corresponding sound power level spectra, PWL, are plotted in Fig. 4. The semi-empirical curves of Heidmann are included for comparison in these figures (their absolute levels are arbitrary).[10] These computations based on the Kirchhoff method are in perfect agreement with the curves of reference 2 using the T&S model, as shown for instance in Fig. 5 at a rotation speed of 7120 rpm (Kirchhoff and Heidmann curves are the same as in Figs. 3 and 4). The only difference is that Kirchhoff directivities better reproduce Heidmann's prediction around 90° because the hypothesis of flanged inlet has not been made. Heidmann's spectra do not agree with the curves of Figs. 4 or 5(b) below the blade passing frequency, but they were also found to be different from the measurements.[9] Discrepancies at lower frequencies may be caused by some additional noise sources, such as vorticity production at the nacelle exit rim.

Overall sound power levels (OAPWL) give an overall view of the results. They can be calculated in two ways: i) Inside the duct, integrating over a cross section the sound intensities of all the propagating modes at each frequency; ii) In the free field, integrating the directivities (or sound power spectra) displayed in Figs. 3 or 4. These two computations should lead to the same OAPWL value. They are compared in Fig. 6 versus the rotation speed (in logarithmic scale) for forward and aft radiation. Either the T&S radiation model (Fig. 6(a)) or the Kirchhoff method (Fig. 6(b)) is used. OAPWL inside the duct are of course identical in the two graphs.

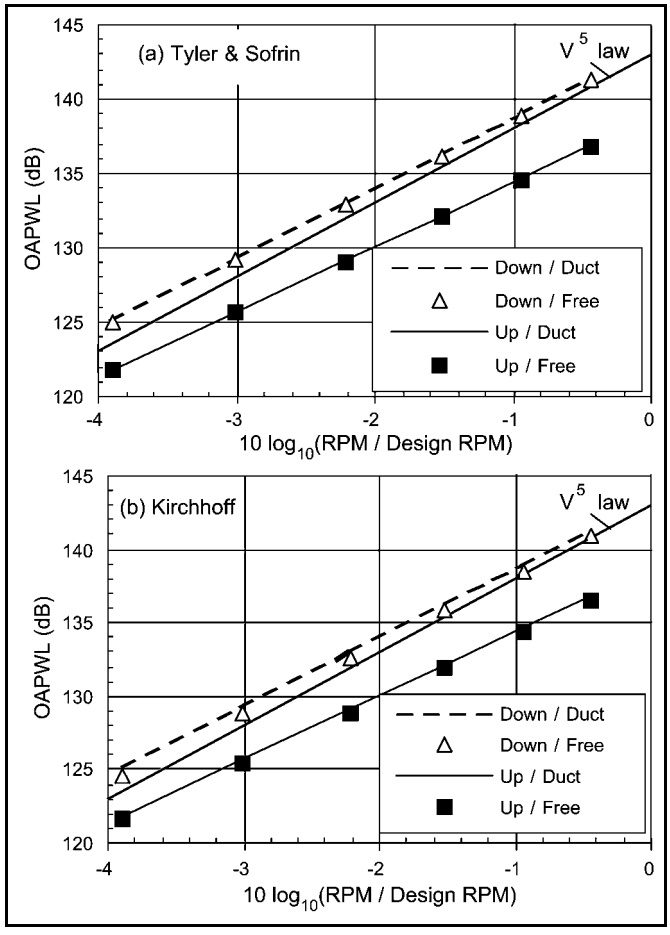


**Figure 6.** Upstream and downstream overall sound power levels, without any flow (straight line in the middle is the law in velocity to the fifth power).

It is confirmed that radiated OAPWL (symbols) are very close to induct OAPWL (black lines), as expected. The differences in the Kirchhoff integral are around 0.3 dB for upstream radiation and 0.6 dB downstream. These free-field OAPWL are slightly lower than those found using T&S, probably because there is no assumption of flanged inlet, and radiation extends over more than 90 degrees in $\theta$. It is also shown in Fig. 6 that sound power increases in velocity to the fifth power, which is the conventional law for a rotating dipole.[11]

It should be noted with respect to the downstream curves that all the computations are related to rotor emission, although actual aft radiation is rather due to the interaction of wakes shed from the blades with the outlet guide vanes.

### 3.2. Flow Effect

Conditions of static tests are considered in Fig. 7, with a uniform flow inside the duct and no flow in free space. Here are plotted as before the forward (Fig. 7(a)) and aft (Fig. 7(b)) overall sound power levels versus the logarithm of rotational speed for the Kirchhoff computation. Results are again nearly the same as in the T&S approach, as is shown in Fig. 8 by the differences among free-field OAPWL (they are less than 0.5 dB). The curves neglecting induct flow (labelled "$M = 0$") are included for comparison (these are the induct results of Fig. 6).

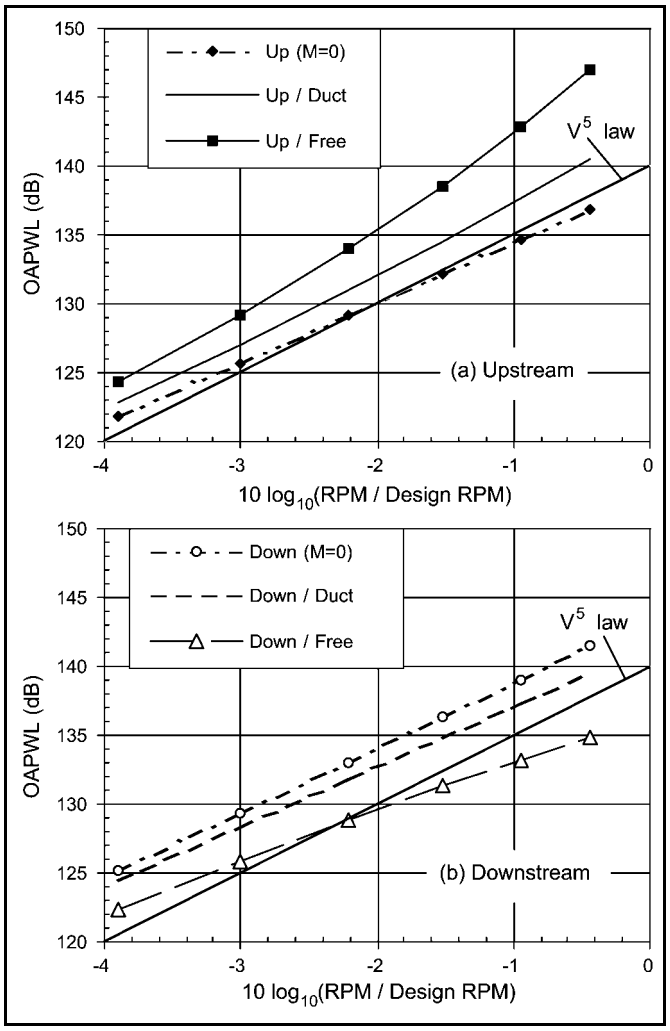


**Figure 7.** Overall sound power level versus rotation speed in static, with induct flow: Kirchhoff computation (straight line from 120 to 140 dB is the law in velocity to the fifth power).

Flow velocity inside the duct (plotted in Fig. 9) tends to increase upstream induct sound power and to decrease downstream sound power. There are however very large discrepancies between induct and free-field OAPWL, reaching more than 5 dB (in absolute value) at high speed, as seen in Fig. 10. Even at low Mach number (about 0.1), differences are around 2 dB. This can be roughly understood by applying Eq. (14) to the axial acoustic intensity inside the duct. Let us take $p/u_z \approx \varepsilon \rho_0 a$ like for plane waves ($\varepsilon = +1$ downstream, $\varepsilon = -1$ upstream). Thus:

$$I_z(M_z) \approx (1 + \varepsilon M_z)^2 I_z(M_z = 0),$$

and

$$\Delta L = 20 \log\left[\frac{I_z(M_z)}{I_z(0)}\right] \approx 20 \log(1 + \varepsilon M_z). \qquad (21)$$

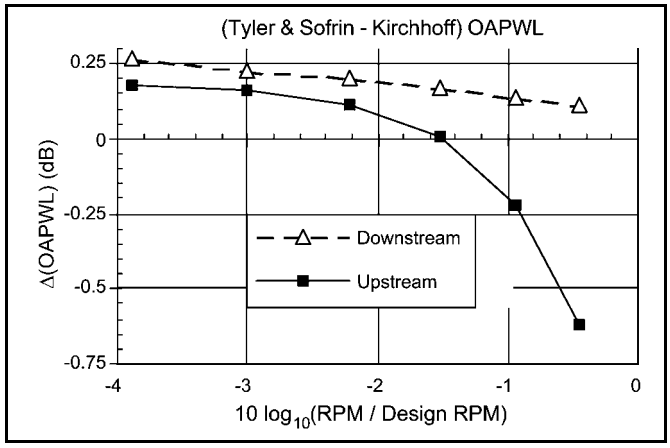


**Figure 8.** Difference in computed free-field radiation versus rotation speed: Static conditions, with induct flow.

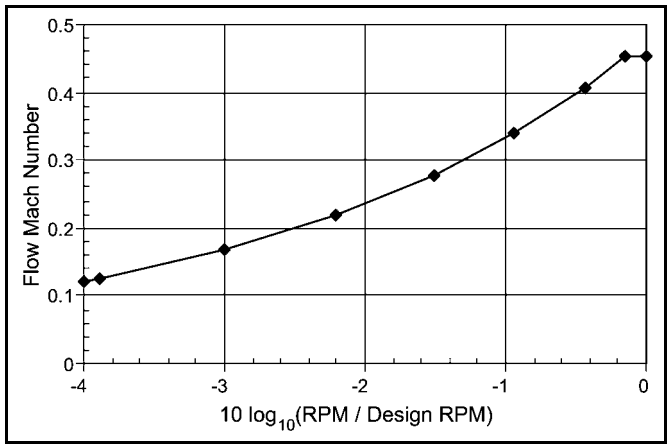


**Figure 9.** Induct flow Mach number.

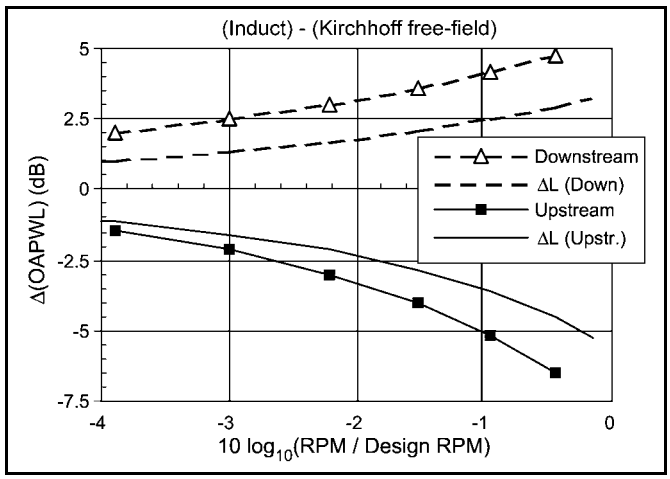


**Figure 10.** Effect of induct flow Mach number on overall sound power levels in static conditions.

This ratio, $\Delta L$, should be of the order of the difference between the power level inside the duct (at $M_z \neq 0$) and in the free field ($M_z = 0$). It is also plotted in Fig. 10 (curves with-

out symbol) and is in fairly good agreement with the above results in spite of the plane-wave approximation.

It is confirmed that these analytical acoustic predictions are not valid if there is a flow mismatch in the duct exit plane, using either the T&S or Kirchhoff method. Although the T&S model is a kind of simplified Kirchhoff integral, these cross-checks between the two methods were not obvious because coefficient $P_0$ in Eq. (10) does not reduce to the analog expression of T&S, even without flow. In this case:

For T&S,

$$P_{0(\mathrm{T\&S})} = \frac{1}{2} A_{m\mu} R k_z \,, \tag{22a}$$

For Kirchhoff,

$$P_{0(\mathrm{K})} = P_{0(\mathrm{T\&S})}\left(\frac{1}{2} + \frac{K}{2k_z}\cos\theta\right). \tag{22b}$$

The last term of Eq. (22b) in parentheses is close to 1 because $k_z$ and $\cos\theta$ have the same sign, and $K$ is greater than $|k_z|$ for propagating modes. Moreover, the direction of maximum radiation is roughly given by ray acoustics:[12]

$$\sin\theta_{\max} \approx k_t/K \,, \text{ or } \cos\theta_{\max} \approx k_z/K \,,$$

and then

$$\left(\frac{1}{2} + \frac{K}{2k_z}\cos\theta_{\max}\right) \approx 1 \,. \tag{23}$$

This helps us to understand why the two methods are similar, but it was important to verify numerically that they lead to nearly identical results. This would appear to be the first time that the T&S model has been cross-checked against the Kirchhoff method.

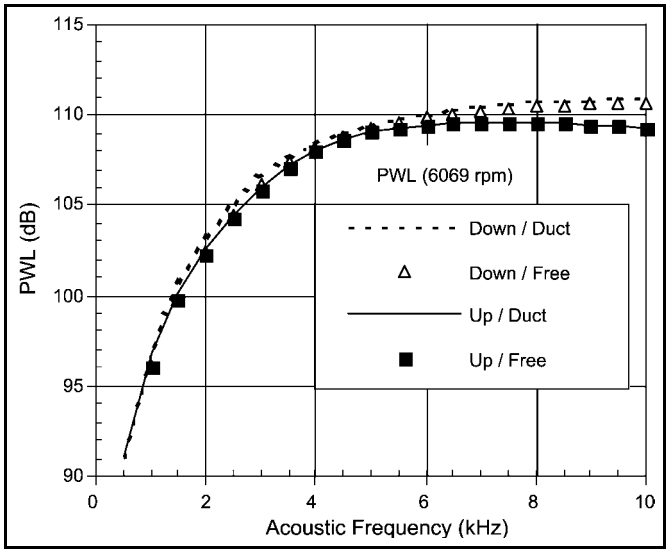


**Figure 11.** Kirchhoff prediction of the sound power spectra at 6069 rpm: Uniform flow throughout the space.

Final results are displayed in Figs. 11 and 12, now assuming the same uniform velocity inside the duct and in the free field. Figure 11 is an example of sound power spectra at a given rotation speed. Figure 12 is like Fig. 7. The curves without flow, and the sound power levels inside the duct are of course the same as before. In this case, an extended T&S computation would be invalid. On the contrary, the free-field power levels using the Kirchhoff integral and Eq. (20) now perfectly collapse on the ducted PWL. As before it can be seen that forward radiation tends to increase with flow, whereas aft radiation tends to decrease. They become approximately equal around transonic tip speeds (abscissa −1), and upstream radiation is stronger at higher speeds.

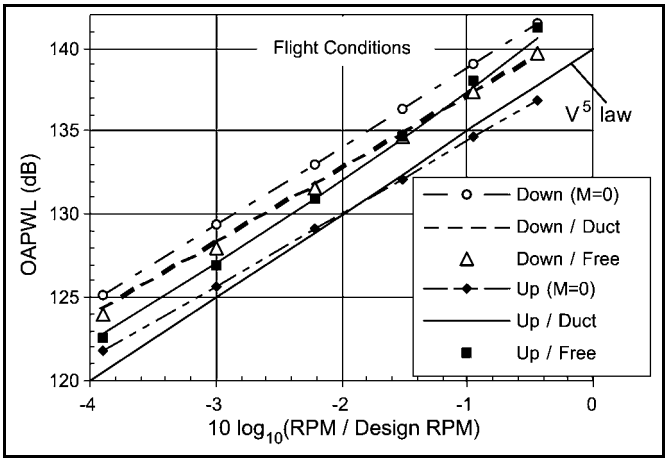


**Figure 12.** Kirchhoff prediction of the overall sound power level versus rotation speed: Uniform flow throughout the space (straight line from 120 to 140 dB is the law in velocity to the fifth power).

## 4. COMPARISON WITH TEST DATA

It can be seen that the variation of OAPWL versus rotation speed is different from the curves of a previous article.[2] This is due to the fact that the blade loading, $F$, was expressed as a function of the angle $\varphi$, and its Fourier transform, $\Phi_s$, was a function of wave-number $s$, such that the source frequency was $f_s = sN$ ($N$ is the rotation speed, and $s$ is a real number, not an integer, for the broadband component). In fact, the blade pressure spectra are assumed to be functions of $f_s$, deduced from the Fourier transform, $\Phi_f$, of the blade loading expressed as a function of the retarded time $\tau$. As $\varphi = 2\pi N\tau$, it comes:

$$F(\tau) = \int_{-\infty}^{+\infty} \Phi_f(f_s) e^{2\pi i f_s \tau} df_s = \int_{-\infty}^{+\infty} \Phi_f(f_s) e^{is\varphi} N ds \,,$$

and thus

$$\Phi_s(s) = N\Phi_f(f_s) \,. \tag{24}$$

The Fourier transform has thus been multiplied by $N$ in this article to be coherent with the previous paper, which means that absolute levels are not the same as before. This however does not change anything on the relative levels at a given rotation speed since $N$ is then a constant. Acoustic spectra and free-field directivities keep the same shapes as before, and comparisons between induct and free-field sound levels, computed using either the Tyler and Sofrin or the Kirchhoff approaches, do not depend on the factor $N$.

All the results shown up to now have been computed for a blade loading in $U_{hel}^2$, the square of the relative fluid velocity on the blades. Let us now consider for validation with test data that:

$$\delta F \propto \pi \rho_0 c U_{hel} v \delta r \,, \tag{25}$$

(the equality being found for a Joukowsky airfoil), where $\rho_0$ is the fluid density, $c$ is the airfoil chord, and $v \approx U_{hel}\alpha$ is the

normal velocity fluctuations ($\alpha$ is the flow angle of attack, in radians). Computations without flow and for a uniform velocity throughout the space are displayed as before in Fig. 13, along with the experimental data from far-field measurements in the upstream anechoic chamber. Angle $\alpha$ decreases as the rotational speed increases towards design speed, and this is the reason why sound levels increase much less than $N^5$ as in the above figures. An approximate law of $\alpha \propto 1/N$ was taken in reference 2 which gave a variation around $N^3$ as shown in Fig. 13. In fact, values of $\alpha$ are here defined more accurately, and the shape of the predicted forward radiation fits the tests much better than before.

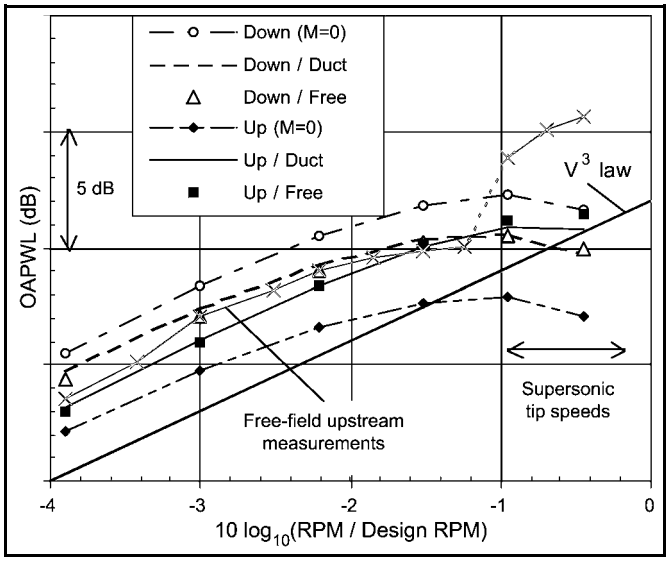


**Figure 13.** Comparison of computed and measured broadband overall sound power levels versus rotation speed (straight line is the law in velocity to the third power).

Three more comments can be made on Fig. 13.

i) The absolute level of the experimental curve is of no significance in this graph because an arbitrary factor of proportionality has been put in Eq. (25) to produce a good fit with the test data. However, the same computations were made on a low-speed fan at the University of Siegen (Germany) for which fore and aft acoustic measurements were available, along with blade pressure measurements.[13] No arbitrary factor was needed, and the predicted sound levels were in fairly good agreement with experiments.

ii) There is a sharp increase in the experimental curve around abscissa $-1$ which corresponds to transonic tip speeds and to the onset of radiation of multiple pure tones (harmonics of the shaft frequency). These could not be well removed from the measured spectra and explain the gap. Some other runs were made by Rolls-Royce with an acoustic lining on the inlet duct wall providing good absorption for these tones, and sound levels were then continuous around transonic tip speeds as in the predictions.

iii) The power law in velocity does not perfectly duplicate the curves. Reduction of experimental broadband spectra in fact showed that:[9]

$$\mathrm{OAPWL\,(dB)} = 50\log(M_{hel}) + 1.6\alpha\,(\mathrm{deg}) + \mathrm{constant}, \quad (26)$$

where $M_{hel}$ is the helical tip Mach number. This was found to be in accordance with other papers on semi-empirical prediction of rotor broadband noise.

## 5. CONCLUSIONS

This work is an extension of a previous article (reference 2). An analytical method was proposed to predict broadband noise radiated by a ducted fan during static tests, i.e., assuming a uniform flow inside the duct and the free-field fluid being at rest. Previous results however neglected the flow velocity in the duct to balance ducted and free-field sound power levels. It has been shown that differences are very large, of several decibels, if there is a flow mismatch on the duct exit.

The simple radiation model of T&S (Rayleigh's integral) has been extended to a complete Kirchhoff integral in order to also take into account a uniform flow in the free field. It has been confirmed as a first step that the two methods give the same results in a medium at rest, either without or with flow inside the duct. This may be the first time that such a verification of the T&S theory has been made.

The new computer code has been used to predict acoustic radiation in a free space at the same velocity as the fluid in the duct. It has been found that sound power levels are then identical in the duct and in the free field, which confirms the validity of the calculations. These "flight conditions" are approximate because the flow velocity in a nacelle is different from the aircraft's forward speed. They however show that it is valid to calculate the sound power inside the nacelle to estimate what would be radiated even if fluid velocity were different in the free space. The main assumption is that there is no reflection on the duct exit, which is more or less true except at low frequencies.

Even if it is expected that computational fluid dynamics will provide the random blade pressure fluctuations in the near future, this method will always hold some interest because numerical data could be entered as input. That would be much more accurate than the generic spectrum used up to now. Moreover, acoustic computations are very fast on a PC, and optimisations of noise sources could be considered through parametric studies.

## REFERENCES


1 Gliebe, P.R. Fan broadband self noise prediction model, AIAA Paper 2002-2490, 8th AIAA/CEAS Aeroacoustics Conference & Exhibit, Breckenridge, CO, (2002).

2 Lewy, S. Computation of broadband noise radiated by a ducted fan, *International Journal of Acoustics and Vibration*, **7** (3), 141-153, (2002).

3 Ffowcs Williams, J.E., and Hawkings, D.L. Theory relating to the noise of rotating machinery, *J. Sound Vib.*, **10** (1), 10-21, (1969).

4 Goldstein, M.E. *Aeroacoustics*, McGraw-Hill International Book Company, New York, (1976).

5 Tyler, J.M., and Sofrin, T.G. Axial flow compressor noise studies, *Society of Automotive Engineers (SAE) Transactions*, **70**, 309-332, (1962).

6 Lewy, S. Overview on fan noise prediction, ONERA Preprint No. 2002-98, Kolloquium für Fluid- und Thermodynamik, Universität Siegen, Germany, (2002).

7 Polacsek, C., and Prieur, J. High-speed impulsive noise computation in hover and forward flight using a Kirchhoff formulation, CEAS/AIAA Paper 95-138, 1st Joint CEAS/AIAA Aeroacoustics Conference, Munich, Germany, (1995).

[8] Cantrell, R.H., and Hart, R.W. Interaction between sound and flow in acoustic cavities: Mass, momentum, and energy considerations, *J. Acoust. Soc. Am*., **36** (4), 697-706, (1964).

[9] Lewy, S. Experimental study of upstream fan broadband noise radiated by a turbofan model, *International Journal of Acoustics and Vibration*, **6** (2), 65-75, (2001).

[10] Heidmann, M.F. Interim prediction method for fan and compressor source noise, NASA Technical Memorandum X-71763, (1st Edition 1975, & 1979).

[11] Ffowcs Williams, J.E., and Hall, L.H. Aerodynamic sound generation by turbulent flow in the vicinity of a scattered half plane, *J. Fluid Mech*., **40** (4), 657-670, (1970).

[12] Rice, E.J. Multimodal far field acoustic radiation pattern using mode cutoff ratio, AIAA Paper 77-1281, AIAA 4th Aeroacoustics Conference, Atlanta, GA, (1977) & *AIAA J*., **16** (9), 906-911, (1978).

[13] Carolus, Th.H., and Stremel, M. Blade surface pressure fluctuations and acoustic radiation from an axial fan rotor due to turbulent inflow, *Acta Acustica united with Acustica*, **88** (4), 472-482, (2002).